ACS OMEGA

http://pubs.acs.org/journal/acsodf

Article

a Versatile Schiff Base Chemosensor for the Determination of Trace Co^{2+}, Ni^{2+}, Cu^{2+}, and Zn^{2+} in the Water and Its Bioimaging Applications

Hongmei Liu, Shangli Ding, Quan Lu, Yue Jian, Gang Wei, and Zeli Yuan*

Cite This: *ACS Omega* 2022, 7, 7585−7594

Read Online

ACCESS | Metrics & More | Article Recommendations | Supporting Information

ABSTRACT: In this work, a simple and versatile Schiff base chemosensor (**L**) was developed for the detection of four adjacent row 4 metal ions (Co^{2+}, Ni^{2+}, Cu^{2+}, and Zn^{2+}) through colorimetric or fluorescent analyses. **L** could recognize the target ions in solutions containing a wide range of other cations and anions. The recognition mechanisms were verified with a Job's plot, HR-MS assays, and ^1H NMR titration experiments. Then, **L** was employed to develop colorimetric test strips and TLC plates for Co^{2+}. Meanwhile, **L** was capable of quantitatively measuring the amount of target ions in tap water and river water samples. Notably, **L** was used for imaging Zn^{2+} in HepG2 cells, zebrafish, and tumor-bearing mice, which demonstrated its potential biological applications. Therefore, **L** can probably serve as a versatile tool for the detection of the target metal ions in environmental and biological applications.

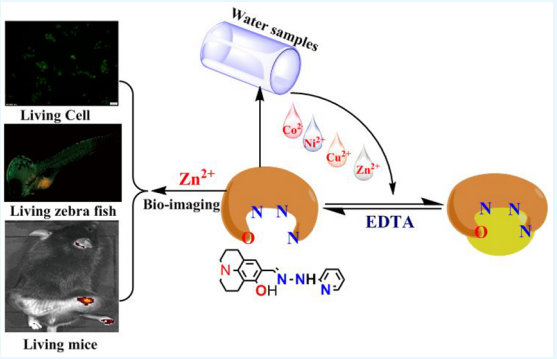

INTRODUCTION

As is known to all, doubly charged metal ions such as Co^{2+}, Ni^{2+}, Cu^{2+}, and Zn^{2+} play important roles in the environment and biologic processes, especially in maintaining human nutrition and health.[1] For instance, an excess of Co^{2+} could lead to vasodilatation and cardiomyopathy,[1c,2] Similarly, an overload of Ni^{2+} would result in asthma, angina, or other cardiac symptoms.[3] Daily intake of Cu^{2+} and Zn^{2+} is required to remain healthy.[4] However, unregulated Cu^{2+} and Zn^{2+} may cause illness. For example, copper deficiency is associated with myelopathy.[4c,d,5] Conversely, the excess intake of Cu^{2+} can adversely affect human health.[1e,2b,5] Non-regulatory Zn^{2+} levels could lead to Alzheimer's disease, epilepsy, etc.[6] Hence, the construction of a feasible method for the detection of the above four adjacent row 4 metal ions (Co^{2+}, Ni^{2+}, Cu^{2+}, and Zn^{2+}) is urgently needed . To date, principal component feed-forward neural networks (PCFFNNs) and feed-forward neural networks (FFNNs) are the only reported methods for the detection of multiple metal ions.[7] However, these methods are based on a series of complexation reactions[7] and therefore suffer from several limitations, such as lengthy sample preparations and complicated calculation procedures.

Among many analytical methods, colorimetric and fluorescent analyses with small molecular chemosensors that can recognize various metal ions simultaneously are of vital importance because of their readily available and rapid operations (Table S1).[7] Compared with the detection of an individual target ion, the exploration of multiple toxic metal ions with a single chemosensor is time- and cost-effective,[7] which maximizes the convenience and economy of an analytical technique.[8] Nevertheless, the development of chemosensors with the ability to detect multiple metal ions is a challenge,[9,10] especially when those ions are adjacent in the periodic table.[9,10]

Chemosensors containing julolidine are usually water-soluble.[11] 2-Hydrazinylpyridine is capable of recognizing metal ions because it can form coordinate bonds with metal ions via its hydrazine group. Therefore, in this work we describe a simple chemosensor (**L**) consisting of the julolidine and 2-hydrazinylpyridine moieties (Scheme 1). The recognition properties of **L** for Co^{2+}, Ni^{2+}, Cu^{2+}, and Zn^{2+} ions were evaluated by colorimetric or fluorescent analyses. Moreover, **L** is able to image Zn^{2+} in live cells, zebrafish, and tumor-bearing mice.

Scheme 1. Synthetic Procedure for L

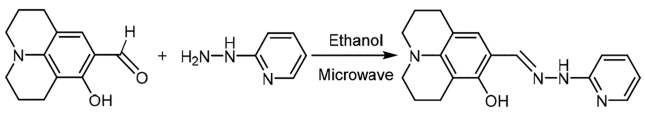

Received: October 28, 2021
Accepted: January 31, 2022
Published: February 28, 2022

RESULTS AND DISCUSSION

The synthetic procedure to target chemosensor **L** is outlined in Scheme 1. In brief, 8-hydroxyjulolidine-9-carboxaldehyde and 2-hydrazinylpyridine were efficiently condensed in methanol under microwave irradiation for 15 min. **L** was perfectly characterized by NMR (^{1}H and ^{13}C), FT-IR, and mass spectrometry (MS) (Figures S1−S4).

The sensing behavior of chemosensor **L** was first investigated by absorption and fluorescence tests with various cations (Li^+, Ag^+, Cd^{2+}, K^+, Ca^{2+}, Na^+, Mg^{2+}, Co^{2+}, Ni^{2+}, Cu^{2+}, Zn^{2+}, Pb^{2+}, Al^{3+}, Ba^{2+}, Fe^{3+}, Sr^{2+}, and La^{3+}) and different anions (CN^-, I^-, SCN^-, NO_3^-, HSO_4^-, SO_4^{2-}, Cl^-, HCO_3^-, CO_3^{2-}, ClO_3^-, PO_4^{3-}, HPO_4^{2-}, $H_2PO_4^-$, $Cr_2O_7^-$, S^{2-}, MoO_4^-, Br^-, and AcO^-) in a 50% ethanol/tris-HCl buffer solution (pH = 7.40) at 25 °C.

After adding different concentrations of cations and anions (detailed above) to the **L** solution, only Cu^{2+} caused a prominent blue-shift in the absorption spectrum. Instead, Co^{2+}, Ni^{2+}, and Zn^{2+} generated a remarkable red-shift in the absorption spectrum (Figures 1 and S5). Moreover, anions

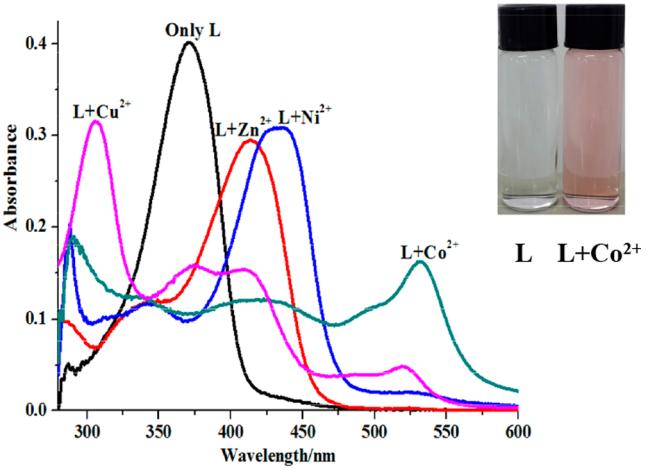

Figure 1. Absorption spectra variation of chemosensor **L** (20 μM) before and after the addition of Co^{2+} (40 μM), Ni^{2+} (40 μM), Cu^{2+} (40 μM), and Zn^{2+} (40 μM) in a 50% ethanol/tris-HCl buffer solution (pH = 7.40). The inset shows the color change of **L** in response to Co^{2+}.

failed to induce any spectral response because of the absence of coordination between **L** and the anions (Figure S6). Besides, among the above four ions that showed obvious spectroscopic responses, only Co^{2+} caused the color of the solution to transform from colorless to wine-colored (Figures 1, S7 ,and S8). This is an increase from the longest spectral red-shift of **L**-Co^{2+} (among these four metal ions), which had a maximum absorption at 532 nm. The unique color transformation of **L** in response to Co^{2+} suggests that **L** could serve as a highly selective colorimetric chemosensor for Co^{2+} detection by the naked eye in aqueous solutions. Taken together, the above results demonstrate that **L** could be utilized as a versatile chemosensor for the synchronous measurement of target ions in aqueous solutions.

The above solutions were also measured by fluorometry with an excitation wavelength of 413 nm. Only Zn^{2+} produced a distinct fluorescence intensity increase at 498 nm (ca. 10×) (Figure 2). By contrast, the fluorescence response for most of the other cations was negligible. The only change was Al^{3+},

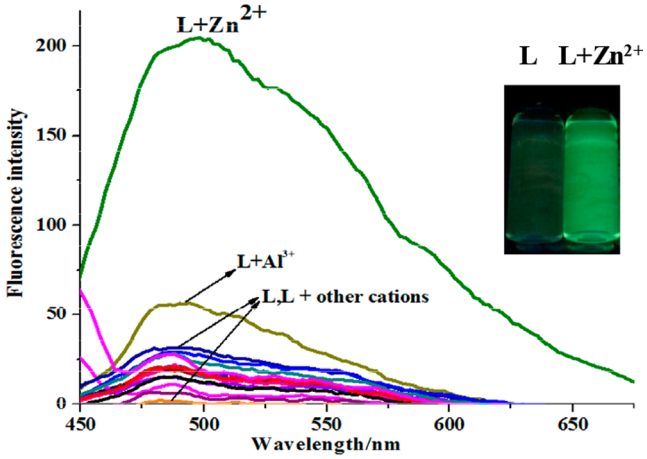

Figure 2. Fluorescence spectra variation of chemosensors **L** (20 μM) before and after the addition of the above-mentioned cations (40 μM), where λ_{ex} = 413 nm. The inset shows the visible fluorescence turn-on of **L** by Zn^{2+}.

which gave an increase 3× the original intensity (Figure 2). Considering the abnormal accumulation of Cu^{2+} under certain illnesses conditions, **L** was also treated with high concentration of Cu^{2+} (200 μM). As shown in Figure S9, Cu^{2+} did not lead to a detectable fluorescence increase even at a high concentration. Moreover, in coexistence of Cu^{2+}, the fluorescence induced by Zn^{2+} decreased slightly and remained constant over at least 1 h (Figure S10). Such a fluorescence decrease could be eliminated by the widely used chelation reagent resin Chelex-100 for Cu^{2+} (*vide infra*), implying that the chelated Cu^{2+} would not interrupt the fluorescence detection of Zn^{2+}. In view of the fact that the intracellular Cu^{2+} is mainly the chelated form,[12] the above results further indicated that **L** is capable of serving as a usable sensor for the fluorescence detection of an abnormal increase in the free Zn^{2+} level in living systems. It is worth mentioning that under UV lamp irradiation at 365 nm, Zn^{2+} could selectively induce the strong blue-green fluorescence of **L**, which could thus be applied for the naked-eye recognition of Zn^{2+} (Figures 2 and S11).

L can "turn on" fluorescence in response to Zn^{2+}, which can be described as a result of the restricted Schiff base group (C═N) isomerization and the excited-state intramolecular proton transfer (ESIPT) mechanism.[13] First, **L** exists as a free ligand in which the rotation of the C═N bond is not restricted. The rotation and isomerization of such an unrestricted C═N bond would act as a nonradiative inactivation process to quench the fluorescence of the fluorogen. Therefore, free **L** has no visible fluorescence. However, when Zn^{2+} is added to **L**, a chelate complex (with an enhanced rigid structure) may form between **L** with Zn^{2+} ion, resulting in the chelation-intensified fluorescence effect.[13] Meanwhile, the intramolecular hydrogen bond (IMHB) between the phenolic O atom of julolidine shows ESIPT,[13a,14] suggesting that the phenol O atom of julolidine could be chelated with Zn^{2+}.[13,14] Therefore, the chelation of Zn^{2+} by **L** may inhibit C═N isomerization and ESIPT, leading to an enhancement of the fluorescence (Scheme 2).

For further studies of the recognition responses between **L** and these four cations, absorption and fluorescence titration experiments were conducted. When **L** was added to increasing amounts of Co^{2+}, Ni^{2+}, Cu^{2+}, or Zn^{2+}, the initial absorption peak of **L** at 370 nm gradually decreased and new peak

https://doi.org/10.1021/acsomega.1c05960
ACS Omega 2022, 7, 7585−7594

Scheme 2. Fluorescence Enhancement Mechanism of L by Zn^{2+} and the Proposed Structure of the L–Zn^{2+} Complex

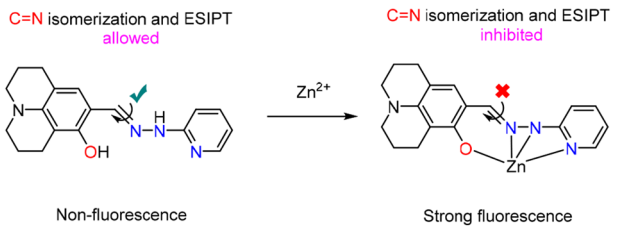

presented. For Co^{2+}, a new absorption peak emerged at 532 nm following the increase of the Co^{2+} concentration from 0 to 20 μM (Figure 3). For Ni^{2+}, a new peak presented at 438 nm,

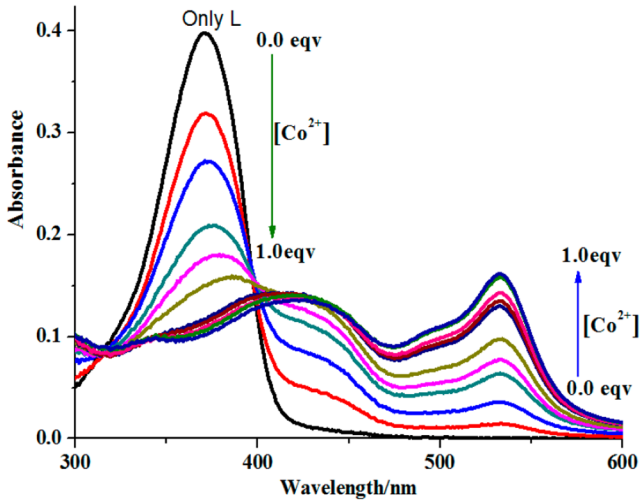

Figure 3. Absorption spectra of chemosensor **L** (20 μM) in the presence of 0–20 μM Co^{2+} in a 50% ethanol/tris-HCl buffer solution (pH = 7.40).

and the absorption intensity gradually increased with the increase of the Ni^{2+} concentration from 0 to 60 μM, reaching its maximum at 60 μM of Ni^{2+} (Figure S12). For Cu^{2+}, three new absorption peak appeared at 306, 416, and 520 nm as the concentration of Cu^{2+} increased from 0 to 400 μM (Figure S13). For Zn^{2+}, an absorption peak emerged at 413 nm as the Zn^{2+} concentration increased from 0 to 100 μM, reaching its maximum at 100 μM of Zn^{2+} (Figure S14). The blue-shift of **L**-Cu^{2+} might be explained by the push–pull effect of the internal charge transfer (ICT) effect.[15] When Cu^{2+} was added to **L**, the chelate complex of **L**–Cu^{2+} was formed through the phenol O, the Schiff base group (C=N) N, and secondary amine (–N–) N atoms complexing with Cu^{2+}, which may have resulted in a feeble push–pull electronic effect. Therefore, the variation of the ICT transition mechanism could be responsible for blue-shift in the absorption spectrum. Meanwhile, the red-shift of the absorption peak shown by **L**–Co^{2+}, **L**–Ni^{2+}, and **L**–Zn^{2+} could be ascribed to ligand-to-metal charge transfer (LMCT) and the ICT effect in the complex formation.[14] The energy gap of the ICT band should decrease upon M^{2+} (M = Co, Ni, and Zn) binding to the electron-donating groups, such as the phenol O atom, the Schiff base group (C=N) N atom, and the secondary amine (–N–) N atom, resulting in the red-shift of **L**–M^{2+}.[16] Moreover, the prominent isoabsorptive points were discovered at 398 nm for Co^{2+}, 397 nm for Ni^{2+}, 328 nm for Cu^{2+}, and 392 nm for Zn^{2+}, which indicated that just one complex was produced from **L** upon binding to Co^{2+}, Ni^{2+}, Cu^{2+}, and Zn^{2+}, respectively. On the other hand, when fluorescence titration was conducted with Zn^{2+}, the fluorescence intensity at 498 nm exhibited its maximum at 40 μM Zn^{2+} (Figure 4). The Job's plots obtained from the absorption

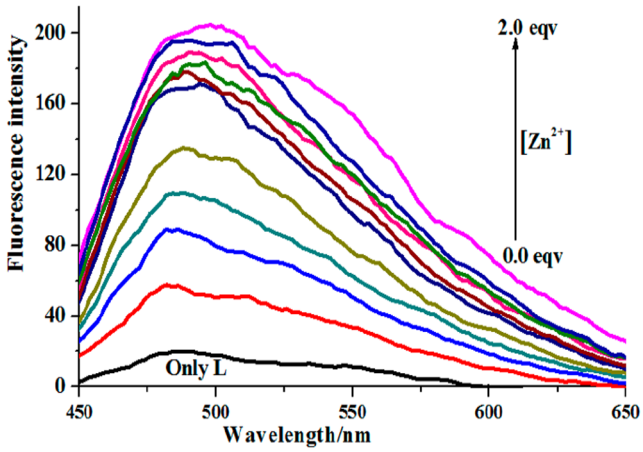

Figure 4. Fluorescence spectra of chemosensor **L** (20 μM) in the presence of 0–40 μM Zn^{2+} in a 50% ethanol/tris-HCl buffer solution (pH = 7.40).

and fluorescence spectrum were applied to confirm the stoichiometry of the formed complexes. Figures 5, S15, and S16 demonstrate the 1:1 stoichiometry of **L** with Cu^{2+}, Zn^{2+}, Co^{2+}, and Ni^{2+}.

The stoichiometry results were further verified by high-resolution mass spectrometry (HR-MS). The HR-MS spectrum of the mixture of **L** with Co^{2+} (Figure 6) shows a peak at m/z 364.2441, which is assigned to $[Co(\mathbf{L})]^{2+}$. Meanwhile, the HR-MS results of the mixtures of **L** with Ni^{2+}, Zn^{2+}, and Cu^{2+} did not show any homologous peaks for $[Ni(\mathbf{L})]^{2+}$, $[Zn(\mathbf{L})]^{2+}$, or $[Cu(\mathbf{L})]^{2+}$. However, the peaks observed in Figures S17–19 at m/z 417.2923, 436.1867, and 438.2 could be attributed to $[Ni(\mathbf{L})(Cl)(H_2O)]^{2+}$, $[Zn(\mathbf{L})(CH_3CH_2OH)(H_2O)]^{2+}$, and $[Cu(\mathbf{L})\ (CH_3CH_2OH)+Na^+]$ (calcd. for 417.0628, 436.1265, and 438.1004), respectively. These study confirmed that **L** formed 1:1 complexes with Co^{2+}, Ni^{2+}, Cu^{2+}, and Zn^{2+}.

To further survey the bonding of chemosensor **L** to Co^{2+}, Ni^{2+}, Cu^{2+}, and Zn^{2+}, ^{1}H NMR titration tests were executed in a 10% D_2O/DMSO-d_6 mixed solvent (Figures 7 and S20–S22). As the concentrations of these metal ions increased, the phenolic –OH proton (Ha, δ 11.19 ppm) and –NH (Hb, δ 10.56 ppm) gradually weakened. The results indicated the complexation of the four metal ions with the phenolic O and N two atoms.[11a,17] Meanwhile, when 1.0 equiv of the metal ion was added into the **L** solution, the phenolic –OH proton and –NH proton almost completely disappeared, indicating 1:1 complexation for $[M(\mathbf{L})]^{2+}$ (M = Co^{2+}, Ni^{2+}, Cu^{2+}, and Zn^{2+}). In addition, the imine proton CH=N (Hc, δ 8.09 ppm) and benzene protons (Hd–Hi, δ 6.63–7.99 ppm) were disturbed and formed broader peaks due to the asymmetry of the $[M(\mathbf{L})]^{2+}$ complexes.[11a,17] Besides, the paramagnetic nature of Cu^{2+}, Co^{2+}, and Ni^{2+} is also a main reason for the quenching of the NMR signals. Therefore, ^{1}H NMR titration experiments not only verified the binding sites of these four metal ions with **L** but also further confirmed the 1:1 complexation of $[M(\mathbf{L})]^{2+}$.

https://doi.org/10.1021/acsomega.1c05960
ACS Omega 2022, 7, 7585–7594

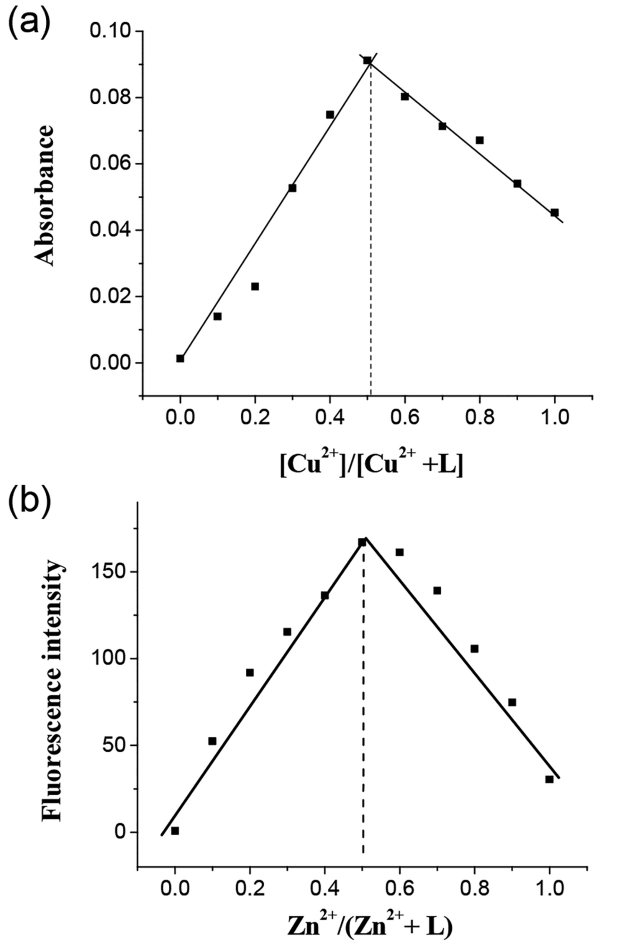

Figure 5. Job's plots for metal ions with **L**. (a) Cu^{2+} (λ_{max} = 306 nm) and (b) Zn^{2+} (λ_{em} = 498 nm), presenting a 1:1 stoichiometry in a 50% ethanol/tris-HCl buffer solution (pH = 7.40).

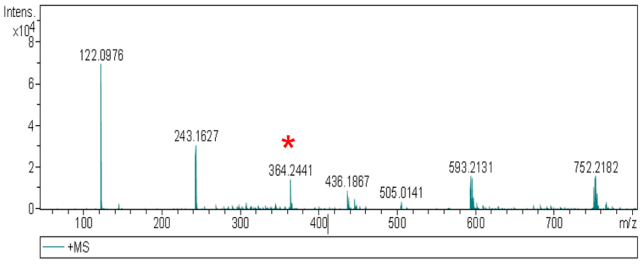

Figure 6. HR-MS spectrum of **L**-Co^{2+} (1.0 eqv) in a 50% ethanol/tris-HCl buffer solution (pH = 7.40).

To study the detection ability of **L** after being recycled for several measurements, the solution of **L** was alternately treated with metal ions and the strong chelating agent EDTA (Figures 8, S23, and S24). The initial absorbances of **L**-Co^{2+}, **L**-Ni^{2+}, **L**-Cu^{2+}, and **L**-Zn^{2+} were recorded at 532, 438, 306, and 413 nm, respectively. After 1.0 equiv of EDTA was added to the **L**−M^{2+} solution, the absorbance of the system prominently decreased. Then, as more metal ions were added to the resulting solution of [**L**−(Co^{2+}/EDTA)], [**L**−(Ni^{2+}/EDTA)], [**L**−(Cu^{2+}/EDTA)], or [**L**−(Zn^{2+}/EDTA)], a recovery of the absorbance or fluorescence was observed. Furthermore, repeated experiments also yielded the same results for at least five cycles. Therefore, these competitive experiments with EDTA further verified the complexation durability of **L** with these four metal ions.

Based on the above-mentioned experiments, the 1:1 complexation structures of **L** with four target ions are proposed in Scheme 3.

The linear relationships between absorption and the concentration of the four metal ions are shown in Figures S25−S28. Meanwhile, the association constants (K_a) of **L** with the four target ions were calculated using the Benesi−Hildebrand equation (Figures S29−S32).[11a,18] The K_a values with **L** were calculated as 1.02×10^5, 1.35×10^5, 1.16×10^5, and 2.10×10^7 M^{-1} for Co^{2+}, Ni^{2+}, Cu^{2+}, and Zn^{2+}, respectively. Furthermore, using $3\sigma/K$ (where σ is the standard deviation of 11 blank absorbances at the detection wavelength shown in Figures S25−S28 and K is the slope of the relative linear equation), the detection limits of **L** were calculated to be 3.20×10^{-8}, 6.00×10^{-8}, 6.23×10^{-7}, and 1.09×10^{-7} M for Co^{2+}, Ni^{2+}, Cu^{2+}, and Zn^{2+}, respectively.

Next, the competitive tests were also performed by adding 2 equiv of 16 cations and 17 anions (as mentioned above) to the **L**−M^{2+} (M = Co^{2+}, Ni^{2+}, Cu^{2+}, or Zn^{2+}) system. The results showed that some metal ions would interfere with the absorption or fluorescence detection of the four metal ions (Figures 9 and S33−S38). For example, in the **L**−Co^{2+} and **L**−Ni^{2+} systems, the coexistence of other metal ions or anions did not influence the response to Co^{2+} and Ni^{2+} by chemosensor **L** expect for Cu^{2+} (Figures 9a and S33−35). However, the application of resin Chelex-100, a widely used chelation reagent for Cu^{2+}, can eliminate the interference of Cu^{2+} for Co^{2+} and Ni^{2+}, which is probably due to the stronger affinity between resin Chelex-100 and Cu^{2+} compared to Co^{2+} and Ni^{2+} (Figures S39 and S40, respectively).[19] Therefore, **L** can serve as a selective chemosensor for the detection of Co^{2+} and Ni^{2+} even with the coexistence of 16 metal ions or 17 anions. For Cu^{2+}, the absorption peak of **L** at 306 nm was not obviously interfered with by the other metal ions or anions except Fe^{3+} and Pb^{2+} (Figures S36 and S37, respectively). However, the interferences from Fe^{3+} and Pb^{2+} can be successfully inhibited using F^- and EDTA, respectively (Figures S41 and S42, respectively). It should be noted that EDTA has comparable affinity to Pb^{2+} and Cu^{2+}[20] but may prefer to form a 1:1 complex with Pb^{2+} to remove its interference in the current system of **L** + Cu^{2+} + Pb^{2+} + EDTA, which is supported by our results. In the case of Zn^{2+}, the fluorescence intensity of **L**−Zn^{2+} suffered from 60% or 90% quenching with the addition of Cu^{2+} or Co^{2+}, respectively (Figure 9b). Fortunately, applications of triethanolamine and the chelating resin Chelex-100 were able to overcome the interferences from Co^{2+} and Cu^{2+} ions, respectively (Figure S43 and S44, respectively).

In addition, we also tested the response time of chemosensor **L** to Co^{2+}, Ni^{2+}, Cu^{2+}, and Zn^{2+} (Figures S45−S47). The results show that **L** can rapidly recognize the four target ions and obtain a stable respond readout in a long time period.

To develop the practical application of **L**, test strips or TLC plates were coated with **L** for the naked-eye detection of Co^{2+} in water. Among the examined metal ions, a prominent color transformation from gray to wine red can be produced by only in the case of Co^{2+} (Figure 10a), implying the selective naked-eye detection of Co^{2+}. In additional, the concentration of Co^{2+} can be quantitatively measured by naked eye using the test strips, and the detection limit was estimated to be 1.0×10^{-5} M. Furthermore, the **L**-coated TLC plates were also sprayed

https://doi.org/10.1021/acsomega.1c05960
ACS Omega 2022, 7, 7585−7594

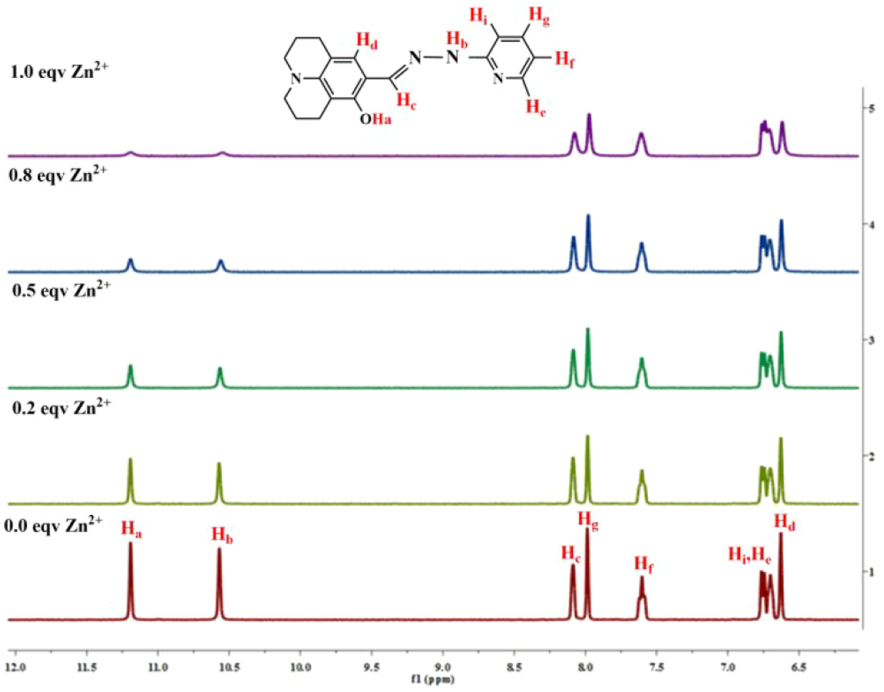

Figure 7. ^{1}H NMR tests of **L** with different concentrations of Zn^{2+} in a mixture of D_2O/DMSO-d_6 (v/v, 1:9).

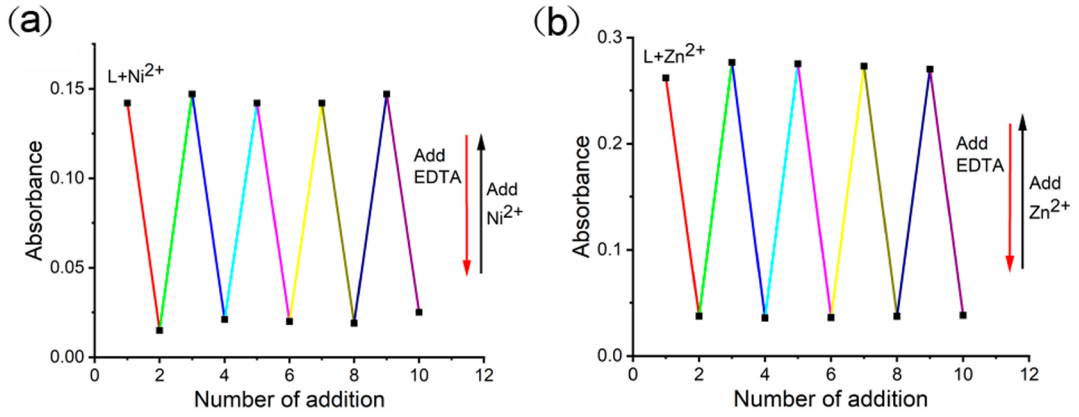

Figure 8. Durability researches of **L** by the alternate treatment of (a) Ni^{2+} or (b) Zn^{2+} and EDTA in 50% ethanol/tris-HCl buffer solution (pH = 7.40).

Scheme 3. Proposed Coordination Mechanism of L−M^{2+} (M^{2+} = Co^{2+}, Ni^{2+}, Cu^{2+}, or Zn^{2+})

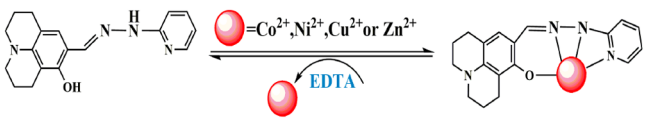

with different concentrations of Co^{2+}. The results show that the **L**-coated TLC plates present an obvious color change from gray to wine, with an estimated detection limit of 1.0×10^{-4} M. Therefore, both **L**-coated test strips and **L**-coated TLC plates could be used for the rapid and easy detection of hazardous Co^{2+} by the naked eye in a real water sample (Figure 10b and c), which may position them as portable tools to be carried and used.

Next, **L** was utilized for the quantitative detection of Co^{2+}, Ni^{2+}, Cu^{2+}, and Zn^{2+} in a variety of water samples such as tap water and river water (Table S2−S5, respectively). At the same time, the detection of Co^{2+}, Ni^{2+}, Cu^{2+}, and Zn^{2+} in environmental water was also performed by ICP-MS assays, which obtained results comparable with those of **L** (Table S6−S9). These results further demonstrate that chemosensor **L** is highly usable in multiple fields such as environmental chemistry and analytical chemistry for the detection of the hazardous Co^{2+}, Ni^{2+}, Cu^{2+}, and Zn^{2+}.

To apply the chemosensor **L** in living cells for the fluorescence imaging detection of Zn^{2+}, we first tested the cytotoxicity of **L** against HepG2 cells using the MTT assay.[21] The results showed that **L** had a low cell inhibitory rate (Figure S48) and could be used as a biocompatible probe for the cellular imaging of Zn^{2+}. As shown in Figure 11, inappreciable fluorescence was found when HepG2 cells were incubated with **L** for 30 min. However, after HepG2 cells were incubated with exogenous Zn^{2+} for other 30 min, strong fluorescence was observed under a fluorescence microscope (IX73). These experimental results indicate that chemosensor **L** is cell-

https://doi.org/10.1021/acsomega.1c05960
ACS Omega 2022, 7, 7585−7594

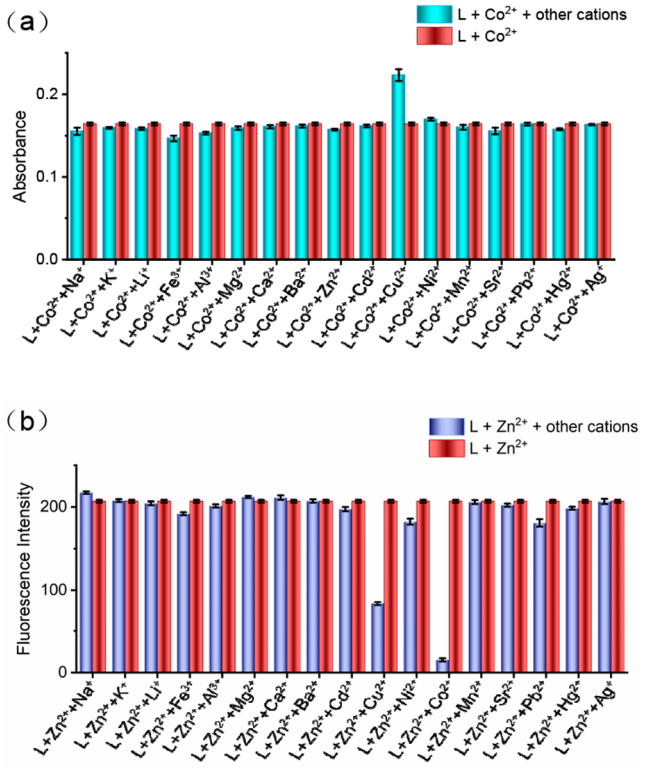

Figure 9. Anti-interference experiments of **L** for metal ions. (a) Absorbance change of **L**−Co^{2+} before and after the addition of other different metal ions (2.0 equiv), where [**L**] = [Co^{2+}] = 20 μM and λ_{max} = 532 nm. (b) Fluorescence intensity of **L**−Zn^{2+} before and after the addition of other different metal ions (2.0 equiv), where [**L**] = [Zn^{2+}] = 20 μM and λ_{em} = 498 nm.

Figure 10. Applications of the 20 μM **L**-coated test strips and TLC plates for the detection of Co^{2+}. (a) The **L**-coated test strips sprayed with 40 μM solutions of different metal ions. (b) The **L**-coated test strips and (c) TLC plates sprayed with different concentrations of Co^{2+} (from left to right: 0.0, 1.0×10^{-6}, 1.0×10^{-5}, 1.0×10^{-4}, 1.0×10^{-3}, 1.0×10^{-2}, and 1.0×10^{-1} M).

penetrable and can serve as a valid candidate for the detection of Zn^{2+} in living cells by fluorescence imaging.

To explore the possibility of detecting Zn^{2+} with **L** in living organisms, we performed fluorescence imaging in zebrafish or tumor-bearing mice. As shown in Figure 12, after being cultured with **L** for 30 min, the zebrafish was observed to have negligible fluorescence. However, the addition of Zn^{2+} to the **L**-loaded zebrafish led to a strong fluorescence enhancement under the fluorescence microscope. These results indicate that **L** could potentially be applied as a chemosensor for monitoring Zn^{2+} accumulation in living organisms.

To further expand the new application field of **L** for imaging Zn^{2+} in live animals, we also established a two-tumor model in C57 mice (one on each side) with B16F10 cells for the fluorescence imaging of Zn^{2+} in the tumors. As shown in Figure 13, it can be seen that the fluorescence signal was not detectable whether the mice were intratumorally injected with PBS (Figure 13a, right) or without PBS (Figure 13a, left), followed by intratumoral injection of Zn^{2+}. Similarly, when only **L** was injected into the tumor, no fluorescence signal was observed (Figure 13b, left). However, the injection of Zn^{2+} resulted in a significant fluorescence increase within 10 min (Figure 13b, right). Overall, these studies indicate that **L** can be applied in live animals to image Zn^{2+}.

CONCLUSIONS

In summary, in this work we reported a simple and versatile chemosensor **L**, which can be used to recognize Co^{2+}, Ni^{2+}, Cu^{2+}, and Zn^{2+} ions. As for as we know, **L** is one of only a few cases of a simple chemosensor capable of sensing four metal ions (Co^{2+}, Ni^{2+}, Cu^{2+}, and Zn^{2+}) that are adjacent on the fourth row of the periodic table. **L** could be used for the quantitative detection of trace amounts of Co^{2+}, Ni^{2+}, Cu^{2+}, and Zn^{2+} in tap water and river water. Particularly, the selective colorimetry determination capacity of **L** for Co^{2+} enables it to be used for the naked-eye monitoring of Co^{2+} levels. More importantly, **L** can also be utilized to image Zn^{2+} in live cells, zebrafish, and tumor-bearing mice, demonstrating its potential application in biological systems. Therefore, **L** is expected to be employed as a simple and versatile chemosensor for the selective detection of environmental and biological traces of Co^{2+}, Ni^{2+}, Cu^{2+}, and Zn^{2+} ions.

EXPERIMENTAL SECTION

All chemicals reagents were of analytical grade and applied without treatment. Double-distilled water was applied for all tests. The NMR tests were performed on an Agilent-400 DD2 spectrometer (Agilent, Palo Alto, CA) in DMSO-d_6 with tetramethylsilane (TMS) as the internal standard. The chemical shifts (δ) were expressed in units of parts per million (ppm) relative to TMS. High-resolution mass spectrometry (HR-MS) experiments were conducted on a time-of-flight Micromass LCT Premier XE spectrometer (McKinley Scientific, Sparta Township, NJ). Fluorescence spectra were recorded on a Cary Eclipse spectrophotometer (Agilent, Palo Alto, CA). UV−vis absorption spectra were recorded on a TU-1901 UV−vis spectrophotometer (PuXi Science and Technology Development Co. Ltd., Beijing, China). IR spectra were recorded on a Vary 1000 FT-IR spectrophotometer (Varian, Palo Alto, CA). Fluorescence images of the cells were obtained by an Olympus IX73+DP73 inverted microscope. Small-animal living imaging was performed on IVIS Lumina LT Series III instrument (Caliper Life Sciences, Hopkinton, MA). Additional experiment procedures are found in the Supporting Information.

Synthesis of Chemosensor L. A mixture of 8-hydroxyjulolidine-9-carboxaldehyde (0.23 g, 1 mmol) and 2-

https://doi.org/10.1021/acsomega.1c05960
ACS Omega 2022, 7, 7585−7594

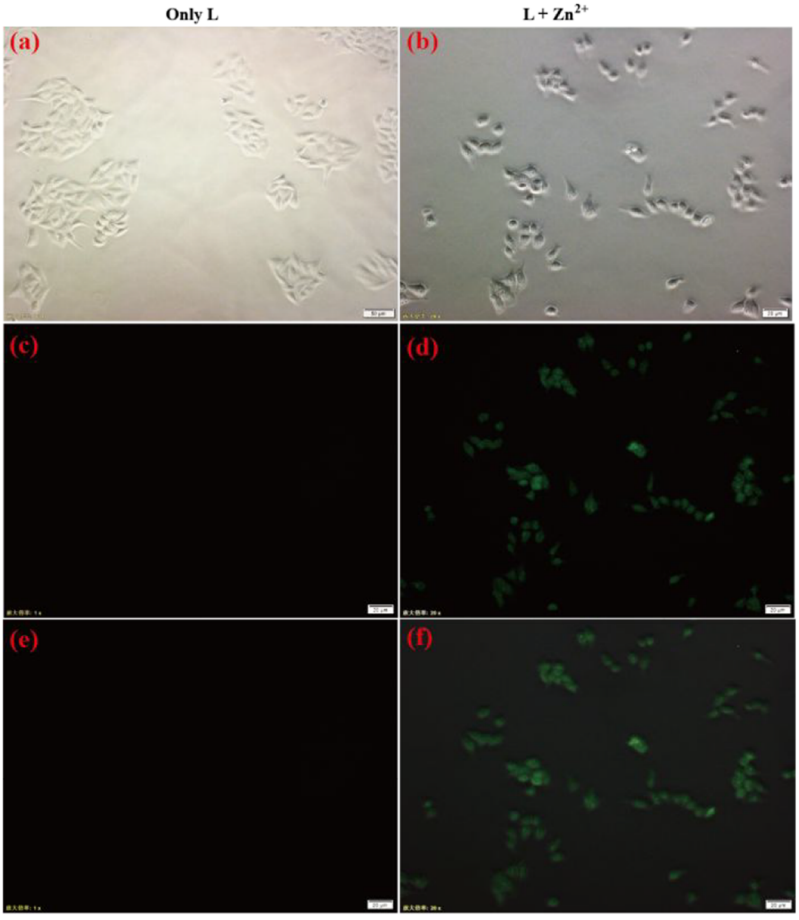

Figure 11. Fluorescence imaging of Zn^{2+} in HepG2 cells with **L**. (a and b) Bright field images. (c and d) Fluorescence images of HepG2 cells treated with (c) **L** or (d) **L** + Zn^{2+}. (e and f) Merged images of (e) panels a and c (f) panels d and b. [**L**] = [Zn^{2+}] = 5 μM, λ_{ex} = 425−485 nm, and λ_{em} = 515 nm.

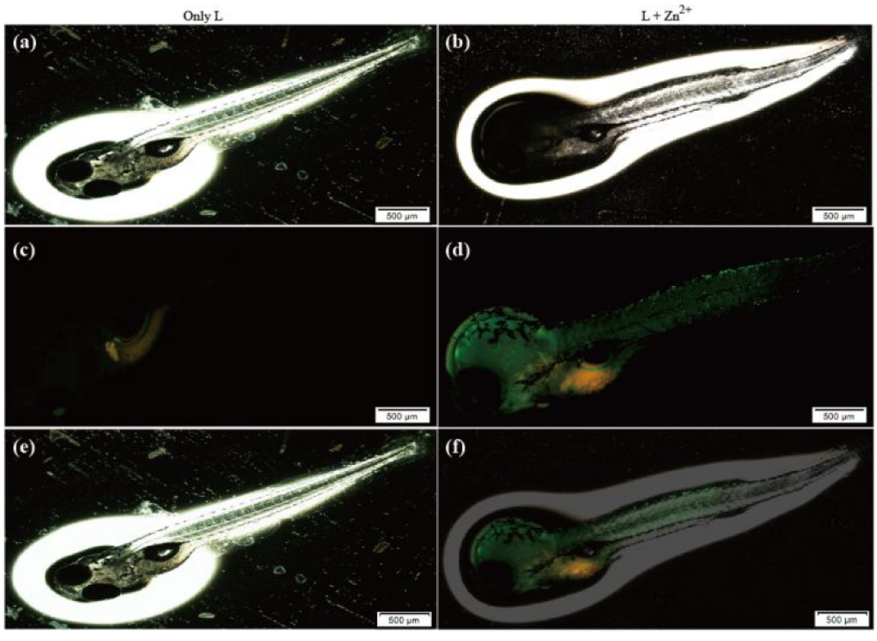

Figure 12. Fluorescence imaging of Zn^{2+} in zebrafish with **L**. (a and b) Bright field images. (c and d) Fluorescence images of zebrafish treated with (c) **L** or (d) **L** + Zn^{2+}. (e and f) Merged images of (e) panels a and c and (f) panels b and d. [**L**] = [Zn^{2+}] = 5 μM, λ_{ex} = 425−485 nm, and λ_{em} = 515 nm.

https://doi.org/10.1021/acsomega.1c05960
ACS Omega 2022, 7, 7585−7594

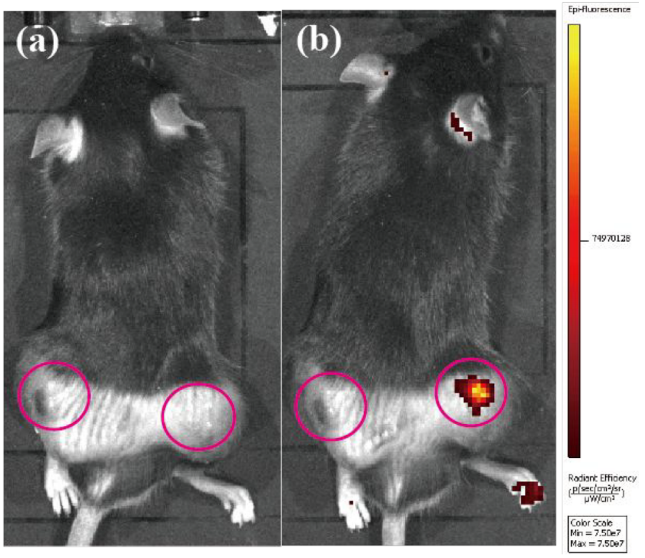

Figure 13. Fluorescence imaging of Zn^{2+} in B16F10 tumor-bearing C57 mice. (a) Fluorescence images of the mice intratumorally injected with only PBS for 10 min (left) and without PBS for 10 min (right), followed by an intratumoral injection of Zn^{2+} on both sides. (b) Fluorescence images of the mice intratumorally injected with **L** on both sides for 10 min, followed by an intratumoral injection of Zn^{2+} on the right side.

hydrazinylpyridine (0.10 g, 1 mmol) in MeOH (25 mL) was irradiated of 300 W at 60 °C for 15 min. After cooling the reaction mixture to an ambient temperature, the formed solid was filtered and washed with cold MeOH and diethyl ether. The crude product was purified by recrystallization from methanol to give 0.32 g of **L** as a yellow solid (85.1%). ^{1}H NMR (DMSO-d_6, 400 MHz) δ (ppm): 1.83(s, 4H, $-CH_2-$), 2.59(s, 4H, $-CH_2-$), 3.11(s, 4H, $-CH_2-$), 6.63(s, 1H, Ar−H), 6.70−6.71 (m, 1H, Ar−H), 6.74−6.76 (d, J = 8.4 Hz, 1H, Ar−H), 7.58 (s, 1H, Ar−H), 7.99 (s, 1H, Ar−H), 8.09(s, 1H, CH═N), 10.58 (s, 1H, NH), 11.20 (s, 1H, OH). ^{13}C NMR (DMSO-d_6, 100 MHz) δ (ppm): 156.20, 153.51, 144.34, 138.21, 127.40, 114.34, 138.21, 127.40, 114.34, 112.55, 107.01, 106.70, 105.53, 26.72, 21.82, 21.06, 20.54. IR (KBr, cm^{-1}) ν: 3445, 2953, 1620, 1545, 1428, 1368, 1307, 1272, 1171, 967, 845, 775, 729. MS(ESI) calcd for $C_{19}H_{20}N_4O_2$ (M + H^+): 310.2. Found: 310.2.

■ ASSOCIATED CONTENT

Supporting Information

The Supporting Information is available free of charge at https://pubs.acs.org/doi/10.1021/acsomega.1c05960.

Additional experiment procedures, spectra (UV−vis absorption, fluorescence, NMR, ESI-MS, and XRD), imaging data, and full reference information(PDF)

■ AUTHOR INFORMATION

Corresponding Author

Zeli Yuan − *Key Laboratory of Basic Pharmacology of Ministry of Education and Joint International Research Laboratory of Ethnomedicine of Ministry of Education, Zunyi, Guizhou Province 563000, China; School of Pharmacy, Zunyi Medical University, Zunyi, Guizhou Province 563000, China; Guizhou International Scientific and Technological Cooperation Base for Medical Photo-Theranostics Technology and Innovative Drug Development, Zunyi, Guizhou Province 563000, China; Key Laboratory of Biocatalysis and Chiral Drug Synthesis of Guizhou Province, Zunyi, Guizhou Province 563000, China; Generic Drug Research Center of Guizhou Province, Zunyi, Guizhou Province 563000, China;* orcid.org/0000-0001-5354-769X; Phone: 86-085128642413; Email: zlyuan@zmu.edu.cn

Authors

Hongmei Liu − *Key Laboratory of Basic Pharmacology of Ministry of Education and Joint International Research Laboratory of Ethnomedicine of Ministry of Education, Zunyi, Guizhou Province 563000, China; School of Pharmacy, Zunyi Medical University, Zunyi, Guizhou Province 563000, China; Guizhou International Scientific and Technological Cooperation Base for Medical Photo-Theranostics Technology and Innovative Drug Development, Zunyi, Guizhou Province 563000, China; Key Laboratory of Biocatalysis and Chiral Drug Synthesis of Guizhou Province, Zunyi, Guizhou Province 563000, China; Generic Drug Research Center of Guizhou Province, Zunyi, Guizhou Province 563000, China*

Shangli Ding − *Key Laboratory of Basic Pharmacology of Ministry of Education and Joint International Research Laboratory of Ethnomedicine of Ministry of Education, Zunyi, Guizhou Province 563000, China; School of Pharmacy, Zunyi Medical University, Zunyi, Guizhou Province 563000, China; Guizhou International Scientific and Technological Cooperation Base for Medical Photo-Theranostics Technology and Innovative Drug Development, Zunyi, Guizhou Province 563000, China; Key Laboratory of Biocatalysis and Chiral Drug Synthesis of Guizhou Province, Zunyi, Guizhou Province 563000, China; Generic Drug Research Center of Guizhou Province, Zunyi, Guizhou Province 563000, China*

Quan Lu − *Key Laboratory of Basic Pharmacology of Ministry of Education and Joint International Research Laboratory of Ethnomedicine of Ministry of Education, Zunyi, Guizhou Province 563000, China; School of Pharmacy, Zunyi Medical University, Zunyi, Guizhou Province 563000, China; Guizhou International Scientific and Technological Cooperation Base for Medical Photo-Theranostics Technology and Innovative Drug Development, Zunyi, Guizhou Province 563000, China; Key Laboratory of Biocatalysis and Chiral Drug Synthesis of Guizhou Province, Zunyi, Guizhou Province 563000, China; Generic Drug Research Center of Guizhou Province, Zunyi, Guizhou Province 563000, China*

Yue Jian − *Key Laboratory of Basic Pharmacology of Ministry of Education and Joint International Research Laboratory of Ethnomedicine of Ministry of Education, Zunyi, Guizhou Province 563000, China; School of Pharmacy, Zunyi Medical University, Zunyi, Guizhou Province 563000, China; Guizhou International Scientific and Technological Cooperation Base for Medical Photo-Theranostics Technology and Innovative Drug Development, Zunyi, Guizhou Province 563000, China; Key Laboratory of Biocatalysis and Chiral Drug Synthesis of Guizhou Province, Zunyi, Guizhou Province 563000, China; Generic Drug Research Center of Guizhou Province, Zunyi, Guizhou Province 563000, China*

Gang Wei − *Commonwealth Scientific and Industrial Research Organization Manufacturing, Lindfield, New South Wales 2070, Australia*

https://doi.org/10.1021/acsomega.1c05960
ACS Omega 2022, 7, 7585−7594

Complete contact information is available at:
https://pubs.acs.org/10.1021/acsomega.1c05960

Notes

The authors declare no competing financial interest.

■ ACKNOWLEDGMENTS

We thank the Natural Science Foundation of China (Grants 81660575 and 82060626), the Innovative Group Project of Guizhou Province of Education (KY[2018]024), the Excellent Youth Scientific Talents of Guizhou ([2021]5638), the Talents of Guizhou Science and Technology Cooperation Platform ([2020]4104), the Guizhou Science and Technology support plan ([2020]4Y158), and the Doctor Foundation of Zunyi Medical University (F-862) for financial support.

■ REFERENCES

(1) (a) Kim, A.; Kang, J. H.; Jang, H. J.; Kim, C. Fluorescent detection of Zn(II) and In(III) and colorimetric detection of Cu(II) and Co(II) by a versatile chemosensor. *J. Indust. Engin. Chem.* **2018**, *65*, 290−299. (b) Anbu, S.; Paul, A.; Surendranath, K.; Solaiman, N. S.; Pombeiro, A. J. A benzimidazole-based new fluorogenic differential/sequential chemosensor for Cu^{2+}, Zn^{2+}, CN^{-}, $P_2O_7^{4-}$, DNA, its live-cell imaging and pyrosequencing applications. *Sens Actuators, B* **2021**, *337*, 129785. (c) Aysha, T. S.; Mohamed, M. B. I.; El-Sedik, M. S.; Youssef, Y. A. Multi-functional colorimetric chemosensor for naked eye recognition of Cu^{2+}, Zn^{2+} and Co^{2+} using new hybrid azo-pyrazole/pyrrolinone ester hydrazone dye. *Dyes Pigm.* **2021**, *196*, 109795. (d) He, X.; Ding, F.; Sun, X.; Zheng, Y.; Xu, W.; Ye, L.; Chen, H.; Shen, J. Reversible chemosensor for bioimaging and biosensing of Zn(II) and pH in cells, larval zebrafish, and plants with dual-channel fluorescence signals. *Inorg. Chem.* **2021**, *60*, 5563−5572. (e) Hishimone, P. N.; Hamukwaya, E.; Uahengo, V. The C2-symmetry colorimetric dye based on a thiosemicarbazone derivative and its cadmium complex for detecting heavy metal cations (Ni^{2+}, Co^{2+}, Cd^{2+}, and Cu^{2+}) collectively, in DMF. *J. Fluoresc.* **2021**, *31*, 999−1008.

(2) (a) An Kim, P.; Lee, H.; So, H.; Kim, C. A chelated-type colorimetric chemosensor for sensing Co^{2+} and Cu^{2+}. *Inorg. Chim. Acta* **2020**, *505*, 119502. (b) Keypour, M. M.; Forouzandeh, F.; Azadbakht, R.; Khanabadi, J.; Moghadam, M. A. Synthesis and characterization of a new piperazine containing macroacyclic ligand and its Cu(II) and Co(II) complexes: An investigation of the ligand's silver specific fluorescent properties. *J. Mol. Struct.* **2021**, *1232*, 130024.

(3) (a) Erten, G.; Karcı, F.; Demirçalı, A.; Söyleyici, S. 1H-pyrazole-azomethine based novel diazo derivative chemosensor for the detection of Ni^{2+}. *J. Mol. Struct.* **2020**, *1206*, 127713. (b) Lu, W.; Chen, J.; Shi, J.; Li, Z.; Xu, L.; Jiang, W.; Yang, S.; Gao, B. An acylhydrazone coumarin as chemosensor for the detection of Ni^{2+} with excellent sensitivity and low LOD: Synthesis, DFT calculations and application in real water and living cells. *Inorg. Chim. Acta* **2021**, *516*, 120144. (c) Kang, J. H.; Lee, S. Y.; Ahn, H. M.; Kim, C. A novel colorimetric chemo-sensor for the sequential detection of Ni^{2+} and CN^{-} in aqueous solution. *Sens. Actuators, B* **2017**, *242*, 25−34.

(4) (a) Mudi, N.; Hazra, P.; Shyamal, M.; Maity, S.; Giri, P. K.; Samanta, S. S.; Mandal, D.; Misra, A. Designed synthesis of fluorescence 'Turn-on' dual sensor for selective detection of Al^{3+} and Zn^{2+} in water. *J. Fluoresc.* **2021**, *31*, 315−325. (b) Hazra, A.; Roy, A.; Mukherjee, A.; Maiti, G. P.; Roy, P. Remarkable difference in Al^{3+} and Zn^{2+} sensing properties of quinoline based isomers. *Dalton Trans.* **2018**, *47*, 13972−13989. (c) Sağırlı, A.; Bozkurt, E. Rhodamine-based arylpropenone azo dyes as dual chemosensor for Cu^{2+}/Fe^{3+} detection. *J. Photochem. Photobiol., A* **2020**, *403*, 112836. (d) He, X. J.; Xie, Q.; Fan, J. Y.; Xu, C. C.; Xu, W.; Li, Y. H.; Ding, F.; Deng, H.; Chen, H.; Shen, J. L. Dual-functional chemosensor with colorimetric/ratiometric response to Cu(II)/Zn(II) ionsand its applications in bioimaging and molecular logic gates. *Dyes Pigm.* **2020**, *177*, 108255. (e) Tang, A.; Yin, Y.; Chen, Z.; Fan, C.; Liu, G.; Pu, S. A multifunctional aggregation-induced emission (AIE)-active fluorescent chemosensor for detection of Zn^{2+} and Hg^{2+}. *Tetrahedron* **2019**, *75*, 130489.

(5) (a) Rahimi, H.; Hosseinzadeh, R.; Tajbakhsh, M. A new and efficient pyridine-2, 6-dicarboxamide-based fluorescent and colorimetric chemosensor for sensitive and selective recogni-tion of Pb^{2+} and Cu^{2+}. *J. Photochem. Photobiol., A* **2021**, *407*, 113049. (b) Trevino, K. M.; Tautges, B. K.; Kapre, R.; Franco, F. C., Jr; Or, V. W.; Balmond, E. I.; Shaw, J. T.; Garcia, J.; Louie, A. Y. Highly sensitive and selective spiropyran-based sensor for Copper(II) quantification. *ACS Omega* **2021**, *6*, 10776−10789. (c) Rha, C. J.; Lee, H.; Kim, C. An effective phthalazine-imidazole-based chemosensor for detecting Cu^{2+}, Co^{2+} and S^{2-} *via* the color change. *Inorg. Chim. Acta* **2020**, *511*, 119788. (d) Pan, W. Y.; Yang, X. Y.; Wang, Y. S.; Wu, L.; Liang, N.; Zhao, L. S. AIE-ESIPT based colorimetric and "OFF-ON-OFF" fluorescence Schiff base sensor for visual and fluorescent determination of Cu^{2+} in an aqueous media. *J. Photochem. Photobiol., A* **2021**, *420*, 113506.

(6) (a) Ghorai, P.; Pal, K.; Karmakar, P.; Saha, A. The development of two fluorescent chemosensors for the selective detection of Zn^{2+} and Al^{3+} ions in a quinoline platform by tuning the substituents in the receptor part: elucidation of the structures of the metal-bound chemosensors and biological studies. *Dalton Trans.* **2020**, *49*, 4758−4773. (b) Sun, A. Q.; Wang, W. X. Adenine deficient yeast: A fluorescent biosensor for the detection of Labile Zn(II) in aqueous solution. *Biosens. Bioelectron.* **2021**, *179*, 113075. (c) Su, Z. Y.; Zhang, H. L.; Gao, Y.; Huo, L.; Wu, Y. G.; Ba, X. W. Coumarin-anchored halloysite nanotubes for highly selective detection and removal of Zn(II). *Chem. Engin. J.* **2020**, *393*, 124695. (d) Ghorui, T.; Hens, A.; Pramanik, K. Synthesis, photophysical properties and theoretical studies of pyrrole-based azoaromatic Zn(II) complexes in mixed aqueous medium. *Inorg. Chim. Acta* **2021**, *527*, 120586.

(7) (a) Afkhami, A.; Abbasi-Tarighat, M.; Khanmohammadi, H. Simultaneous determination of Co^{2+}, Ni^{2+}, Cu^{2+} and Zn^{2+} ions in foodstuffs and vegetables with a new Schiff base using artificial neural networks. *Talanta* **2009**, *77*, 995−1001. (b) Rasouli, Z.; Hassanzadeh, Z.; Ghavami, R. Application of a new version of GA-RBF neural network for simultaneous spectro-photometric determination of Zn(II), Fe(II), Co(II) and Cu(II) in real samples: An exploratory study of their complexation abilities toward MTB. *Talanta* **2016**, *160*, 86−98. (c) Pothulapadu, C. A. S.; Jayaraj, A.; N, S.; Priyanka, R. N.; Sivaraman, G. Novel benzothiazole-based highly selective ratio-metric fluorescent turn-on sensors for Zn^{2+} and colorimetric chemosensors for Zn^{2+}, Cu^{2+}, and Ni^{2+} ions. *ACS Omega* **2021**, *6*, 24473−24483. (d) Li, W.; Jiang, C.; Lu, S.; Wang, F.; Zhang, Z.; Wei, T.; Chen, Y.; Qiang, J.; Yu, Z.; Chen, X. A hydrogel microsphere-based sensor for dual and highly selective detection of Al3+ and Hg2+. *Sens. Actuators, B* **2020**, *321*, 128490. (e) Wang, F.; Wang, K.; Kong, Q.; Wang, J.; Xi, D.; Gu, B.; Lu, S.; Wei, T.; Chen, X. Recent studies focusing on the development of fluorescence probes for zinc ion. *Coord. Chem. Rev.* **2021**, *429*, 213636. (f) Chen, Y.; Wei, T.; Zhang, Z.; Chen, T.; Li, J.; Qiang, J.; Lv, J.; Wang, F.; Chen, X. A benzothiazole-based fluorescent probe for ratiometric detection of Al^{3+} in aqueous medium and living cells. *Ind. Eng. Chem. Res.* **2017**, *56*, 12267−12275.

(8) (a) Xu, J. B.; Liu, N.; Hao, C. W.; Han, Q. Q.; Duan, Y. L.; Wu, J. A novel fluorescence "on-off-on" peptide-based chemosensor for simultaneous detection of Cu^{2+}, Ag^{+} and S^{2-}. *Sens Actuators, B* **2019**, *280*, 129−137. (b) Li, H. Q.; Sun, X. Q.; Zheng, T.; Xu, Z. X.; Song, Y. X.; Gu, X. H. Coumarin-based multi-functional chemosensor for arginine/lysine and Cu^{2+}/Al^{3+} ions and its Cu^{2+} complex as colorimetric and fluorescent sensor for biothiols. *Sens Actuators, B* **2019**, *279*, 400−409. (c) Liu, S. T.; Tan, S.; Hu, H.; Chen, Z.; Pu, S. Z. Novel colorimetric and fluorescent chemosensor for Hg^{2+}/Sn^{2+} based on a photochromic diarylethene with a styrene- linked pyrido[2, 3-b]pyrazine unit. *J. Photochem. Photobiol., A* **2021**, *418*, 113439.

(9) (a) Qin, B.; Zhang, X. Y.; Qiu, J. J.; Gahungu, G.; Yuan, H. Y.; Zhang, J. P. Water- robust zinc-organic framework with mixed nodes

and its handy mixed-matrix membrane for highly effective luminescent detection of Fe^{3+}, CrO_4^{2-}, and $Cr_2O_7^{2-}$ in aqueous solution. *Inorg. Chem.* **2021**, *60*, 1716−1725. (b) Ding, Y. J.; Zhao, C. X.; Zhang, P. C.; Chen, Y. H.; Song, W. W.; Liu, G. L.; Liu, Z. C.; Yun, L.; Han, R. Q. A novel quinoline derivative as dual chemosensor for selective sensing of Al^{3+} by fluorescent and Fe^{2+} by colorimetric methods. *J. Mol. Struct.* **2021**, *1231*, 129965.

(10) (a) Zhang, Q. Y.; Wong, K. M. C. Photophysical, ion-sensing and biological properties of rhodamine-containing transition metal complexes. *Coord. Chem. Rev.* **2020**, *416*, 213336. (b) Paderni, D.; Giorgi, L.; Fusi, V.; Formica, M.; Ambrosi, G.; Micheloni, M. Chemical sensors for rare earth metal ions. *Coord. Chem. Rev.* **2021**, *429*, 213639.

(11) (a) Yang, J.; Yuan, Z. L.; Yu, G. Q.; He, S. L.; Hu, Q. H.; Wu, Q.; Jiang, B.; Wei, G. Single chemosensor for double analytes: spectrophotometric sensing of Cu^{2+} and fluorogenic sensing of Al^{3+} under aqueous conditions[J]. *J. Fluoresc.* **2016**, *26*, 43−51. (b) Paisuwan, W.; Lertpiriyasakulkit, T.; Ruang pornvi-suti, V.; Sukwattanasinitt, M.; Ajavakom, A. 8-Hydroxyjulolidine aldimine as a fluorescent sensor for the dual detection of Al^{3+} and Mg^{2+}. *Sensing and Bio-Sensing Res.* **2020**, *29*, 100358. (c) Zhang, S. Q.; Zhang, Y.; Zhao, L. H.; Xu, L. L.; Han, H.; Huang, Y. B.; Fei, Q.; Sun, Y.; Ma, P. Y.; Song, D. Q. A novel water-soluble near-infrared fluorescent probe for monitoring mitochondrial viscosity. *Talanta* **2021**, *233*, 122592.

(12) Rae, T. D.; Schmidt, P. J.; Pufahl, R. A.; Culotta, V. C.; O'Halloran, T. V. Undetectable intracellular free copper: the requirement of a copper chaperone for superoxide dismutase. *Science* **1999**, *284*, 805−808.

(13) (a) Park, G. J.; Na, Y. J.; Jo, H. Y.; Lee, S. A.; Kim, A. R.; Noh, I.; Kim, C. A single chemosensor for multiple analytes:fluorogenic detection of Zn^{2+} and OAc^- ions in aqueous solution, and an application to bioima aging. *New. J. Chem.* **2014**, *38*, 2587−2594. (b) Wu, J. S.; Liu, W. M.; Zhuang, X. Q.; Wang, F.; Wang, P. F.; Tao, S. L.; Zhang, X. H.; Wu, S. K.; Lee, S. T. Fluorescence turn on of coumarin derivatives by metal cations: a new signaling mechanism based on C = N isomerization. *Org. Lett.* **2007**, *9*, 33−36. (c) Maity, D.; Govindaraju, T. Naphthaldehyde-urea/thiourea conjugates as turn-on fluorescent probes for Al^{3+} based on restricted C = N isomerization. *Eur. J. Inorg. Chem.* **2011**, *2011*, 5479−5485.

(14) (a) Chen, W. H.; Xing, Y.; Pang, Y. A highly selective pyrophosphate sensor based on ESIPT turn-on in water. *Org. Lett.* **2011**, *13*, 1362−1365. (b) Jang, Y. K.; Nam, U. C.; Kwon, H. L.; Hwang, I. H.; Kim, C. A selective colorimetric and fluorescent chemosensor based-on naphthol for detection of Al^{3+} and Cu^{2+}. *Dyes Pigm.* **2013**, *99*, 6−13.

(15) (a) Jo, T. G.; Na, Y. J.; Lee, J. J.; Lee, M. M.; Lee, S. Y.; Kim, C. A multifunctional colorimetric chemosensor for cyanide and copper-(II) ions. *Sens. Actuators, B* **2015**, *211*, 498−506. (b) Park, G. J.; Park, D. Y.; Park, K. M.; Kim, Y.; Kim, S. J.; Chang, P. S.; Kim, C. Solvent-dependent chromogenic sensing for Cu^{2+} and fluorogenic sensing for Zn^{2+} and Al^{3+}: a multifunctional chemosensor with dual-mode. *Tetrahedron* **2014**, *70*, 7429−7438.

(16) (a) Park, G. J.; Hwang, I. H.; Song, E. J.; Kim, H.; Kim, C. A colorimetric and fluorescent sensor for sequential detection of copper ion and cyanide. *Tetrahedron* **2014**, *70*, 2822−2828. (b) You, G. R.; Lee, J. J.; Choi, Y. W.; Lee, S. Y.; Kim, C. Experimental and theoretical studies for sequential detection of copper(II) and cysteine by a colorimetric chemosensor. *Tetrahedron* **2016**, *72*, 875−881. (c) Gunnlaugsson, T.; Leonard, J. P.; Murray, N. S. Highly selective colorimetric naked-eye Cu(II) detection using an azobenzene chemosensor. *Org. Lett.* **2004**, *6*, 1557−1560. (d) Huang, J.; Xu, Y.; Qian, X. A red-shift colorimetric and fluorescent sensor for Cu^{2+} in aqueous solution: unsymmetrical 4, 5-diaminonaphthalimide with NH deprotonation induced by metal ions. *Org. Biomol. Chem.* **2009**, *7*, 1299−1303.

(17) (a) Pankaj, A.; Tewari, K.; Singh, S.; Singh, S. P. Waste candle soot derived nitrogen doped carbon dots based fluorescent sensor probe: An efficient and inexpensive route to determine Hg(II) and Fe(III) from water. *J. Environ. Chem. Engin.* **2018**, *6*, 5561−5569. (b) Lee, Y. J.; Lim, C.; Suh, H.; Song, E. J.; Kim, C. A multifunctional sensor: Chromogenic sensing for Mn^{2+} and fluorescent sensing for Zn^{2+} and Al^{3+}. *Sens. Actuators, B* **2014**, *201*, 535−544.

(18) (a) Mikata, Y.; Yamashita, A.; Kawamura, A.; Konno, H.; Miyamoto, Y.; Tamotsu, S. Bisquinoline-based fluorescent zinc sensors. *Dalton Trans.* **2009**, 3800−3806. (b) Yu, G. Q.; Cao, Y. P.; Liu, H. M.; Wu, Q.; Hu, Q. H.; Jiang, B.; Yuan, Z. L. A spirobenzopyran-based multifunctional chemosensor for the chromogenic sensing of Cu^{2+} and fluorescent sensing of hydrazine with practical applications. *Sens. Actuators, B* **2017**, *245*, 803−814. (c) Sudheer; Kumar, V.; Kumar, P.; Gupta, R. Detection of Al^{3+} and Fe^{3+} ions by nitrobenzoxadiazole bearing pyridine-2, 6-dicarboxamide based chemosensors: Effect of solvents on detection. *New J. Chem.* **2020**, *44*, 13285−13294. (d) Cao, Y.-P.; Wu, Q.; Hu, Q.-H.; Yu, G.-Q.; Yuan, Z.-L. A sensitive probe for detection of Ca^{2+}, Cu^{2+} and Zn^{2+} based on schiff base derivative and application in bioimaging. *Chin. J. Anal. Chem.* **2019**, *49*, 38−48.

(19) (a) Baffi, F.; Cardinale, A. Improvements in use of Chelex-100 resin for determination of copper, cadmium and iron in sea water. *Int. J. Environ. Anal. Chem.* **1990**, *41*, 15−20. (b) Ryan, D. K.; Weber, J. H. Comparison of chelating agents immobilized on glass with chelex 100 for removal and preconcentration of trace copper (II). *Talanta* **1985**, *32*, 859−863.

(20) (a) Choi, D. W.; Zea, C. J.; Do, Y. S.; Semrau, J. D.; Antholine, W. E.; Hargrove, M. S.; Pohl, N. L.; Boyd, E. S.; Geesey, G. G.; Hartsel, S. C.; Shafe, P. H.; McEllistrem, M. T.; Kisting, C. J.; Campbell, D.; Rao, V.; de la Mora, A. M.; DiSpirito, A. A. Spectral, kinetic, and thermodynamic properties of Cu (I) and Cu (II) binding by methanobactin from Methylosinus trichosporium OB3b. *Biochemistry* **2006**, *45*, 1442−1453. (b) López, M. L.; Peralta-Videa, J. R.; Benitez, T.; Duarte-Gardea, M.; Gardea-Torresdey, J. L. Effects of lead, EDTA, and IAA on nutrient uptake by alfalfa plants. *J. Plant Nutr.* **2007**, *30*, 1247−1261.

(21) (a) Qu, X. F.; Yuan, F. M.; He, Z. Q.; Mai, Y. H.; Gao, J. M.; Li, X. M.; Yang, D. Z.; Cao, Y. P.; Li, X. F.; Yuan, Z. L. A rhodamine-based single-molecular theranostic agent for multiplefunctionality tumor therapy. *Dyes Pigm.* **2019**, *166*, 72−83. (b) Mai, Y. H.; Qu, X. F.; Ding, S. L.; Lv, J. J.; Li, X. M.; Gao, P. Y.; Liu, Y.; Yuan, Z. L. Improved IR780 derivatives bearing morpholine group as tumor-targeted therapeutic agent for near-infrared fluorescence imaging and photodynamic therapy. *Dyes Pigm.* **2020**, *177*, 107979. (c) Lv, J. J.; Song, W. T.; Li, X. M.; Gao, J. M.; Yuan, Z. L. Synthesis of a new phenyl chlormethine-quinazoline derivative, a potential anti-cancer agent, induced apoptosis in hepatocellular carcinoma through mediating Sirt1/Caspase 3 signaling pathway. *Front. Pharmacol.* **2020**, *11*, 911.

https://doi.org/10.1021/acsomega.1c05960
ACS Omega 2022, 7, 7585−7594